Appl. Phys. A 87, 47–55 (2007)
DOI: 10.1007/s00339-006-3852-1

Applied Physics A
Materials Science & Processing

S. BARCIKOWSKI[1]
A. HAHN[1]
A.V. KABASHIN[2]
B.N. CHICHKOV[1,✉]

Properties of nanoparticles generated during femtosecond laser machining in air and water

[1] Laser Zentrum Hannover e.V., Hollerithallee 8, 30419 Hannover, Germany
[2] Engineering Physics Department, Ecole Polytechnique de Montreal, Case Postale 6079, Succ. Centre-ville, Montreal, Quebec, H3C3A7, Canada

Received: 25 July 2006/Accepted: 2 December 2006
Published online: 1 February 2007 •

ABSTRACT Femtosecond laser ablation is used to generate nanoparticle aerosols and colloids from solid targets of various materials (Ti, Ag, Au, Co, etc.) in air and water ambience. We determine the influence of different laser parameters (pulse energy, pulse overlap) and properties of media (air, airbrush, water) on the rate of production and size distribution of the laser-generated nanoparticles. It is shown that the pulse overlap and laser fluence are the parameters determining the nanoparticle size. At optimum conditions the nanoparticle productivity can be increased by 150–300%. The generation of multimaterial nanoparticle dispersions is demonstrated. Being free of toxic impurities, the laser-produced nanoparticles may be promising for biomedical applications.

PACS 79.20.Ds; 81.16.Mk; 81.16.-c; 52.38.Ph; 06.60.Jn

1 Introduction

Due to their size-specific and unique properties, nanoparticulate materials and composites have become increasingly popular, promising a breakthrough in the development of novel methods in biosensing, medical diagnostics and therapeutics, cosmetics coatings, etc. [1]. However, application prospects of conventional chemically synthesized nanomaterials are often complicated because of their toxicity, caused by contamination with chemical precursors or additives during their synthesis procedures [2].

Laser ablation has shown itself as an alternative physical nanofabrication method, which offers novel opportunities to solve the toxicity problem. The method consists in the ablation of a target (mostly solid) by intense laser radiation, leading to an ejection of its constituents and the formation of nanoclusters/nanostructures. Such a method permits both nanostructuring of surfaces [3–12] and the synthesis of nanostructures in the vapor state (for a review, see e.g. [13]). In particular, when the target is ablated in vacuum or in a residual gas, the vaporized nanoclusters can be deposited on a substrate, placed at some distance from the target, to form a thin nanostructured film [14–17]. In contrast, the ablation in a liquid ambience (e.g. in aqueous solutions) causes a release of nanoclusters to the environment to form a colloidal nanoparticle solution [18–28]. When performed in a clean, well-controlled environment such as deionized water or aqueous biocompatible solutions, laser ablation realizes the production of ultra-pure nanomaterials with novel surface chemistry, not reproducible by any other method [26–28]. Furthermore, the method does not involve any toxic substances and allows the functionalization of the nanoparticle surface, which makes the laser-synthesized nanoparticles unique for biosensing and imaging in in vivo applications [27].

It is accepted that the efficient production of nanoparticles/nanostructures is achieved due to a natural property of laser–matter interaction to eject material in the form of atoms and further condensation/agglomeration in the gas phase [29–31]. Nanoclusters and nanoparticles can be formed for almost all parameters of applied laser radiation, although larger microscale fragments or droplets can be present due to melting and detachment of microspikes, formed on the target surface as a result of a multipulse illumination [32, 33].

The initial ablation process determines the ablation mass and the temperature of the ejected species, which are decisive for the cluster condensation and growth. In fact, in the first approximation the process can be described by the classical theory of condensation and nucleation in a vapor layer, which distinguishes several phases of the nanocluster growth [34, 35]: nucleation, kinetics-controlled growth, diffusion-controlled growth and finally Ostwald ripening related to the coalescence or fusion of two nanoparticles. In this case, the final size of the nanoparticles is mainly determined by the competition of coalescence and agglomeration processes during the last phase. The fine tuning of nanocluster sizes has been observed during UV laser ablation [13]. In general, one can distinguish three main factors, which can influence size and composition of nanoparticles/nanostructures produced by laser ablation.

1. Properties of laser radiation. Intensity, pulse length and radiation wavelength determine the temperature, density and angular distribution of ejected atoms and particles.
2. Properties of ablated material (absorption at a particular wavelength; melting, evaporation and crystallization temperatures; possibility of chemical modifications).
3. Properties of environment (vacuum, air, water), which affect the cooling rate or may quench the nanoparticle growth.

✉ Fax: +49 511 2788100, E-mail: ch@lzh.de

It is clear that application prospects of laser ablation-based nanofabrication strongly depend on the cost and flexibility of the method. In our opinion, important data on these parameters can be obtained if we consider the process in standard conditions of laser machining in ambient air or water, when no artificial method of nanoparticle size control is applied. Since the mechanism and conditions of radiation absorption are mainly determined by the wavelength and pulse length, it is especially important to know how these parameters affect the final characteristics of nanostructures. As examples, Figs. 1 and 2 show the size distributions of nanoparticles produced by continuous-wave CO_2 laser ablation of various polymers and metals in ambient air. As shown in Fig. 1, more than 90 wt. % of the polymer-based aerosols have diameters smaller than 1 μm. Here, for the majority of the studied polymers, submicron particles in the range of 150–450 nm are generated, whereas CO_2 laser processing of polystyrene (PS) and acrylic polymer (PMMA) predominantly generates nanoparticles with a mass frequency maximum at 90 nm (PS) and 50 nm (PMMA) [36, 37]. Note that these data on polymers are consistent with their properties to decompose and then resolidify. Here, the difference of nanoparticle parameters for polymers is explained by the different macromolecular structure of each polymer and different efficiency of generation of solidified nanoparticles relatively to the production of volatile organic compounds in the gas phase [38–40]. In general, polymers, which release the highest ratio of gases to particles, generate the smallest particles during laser ablation, like PMMA and PS, which release about 90% gases (mainly the monomer) and 10% aerosols with an average diameter below 100 nm, compared to polycarbonate (PC), which releases 95% aerosols with a higher aerodynamic diameter.

As shown in Fig. 2, most of the metal particles (about 90%) produced by CO_2 laser ablation of titanium and ferric alloys in air are also smaller than 1 μm (aerodynamic diameter). They exist as primary particles or as agglomerates. The smallest single particles have geometric diameters of about 5 nm to 10 nm. The relative mass frequency maximum is in the range of 50 to 200 nm.

It should be noted that laser cutting of metals causes the highest rates of total particulate matter (> 20 mg/s), whereas welding, cladding and applications of material removal show typical rates between 1 and 20 mg/s. For laser cutting of polymers and metals, the primary particles show a spherical shape. As can be seen in the scanning electron microscopy (SEM) pictures in Figs. 1 and 2, the particles generated during this thermal laser ablation process tend to aggregate and agglomerate.

In spite of the differences in pulse lengths and absorption mechanisms for infrared (Nd:YAG and CO_2) lasers, resulting

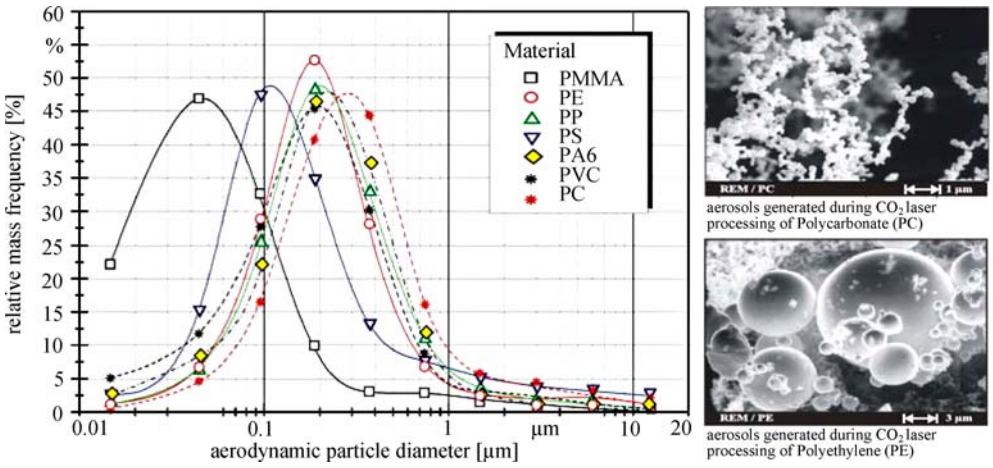

FIGURE 1 Size distributions and SEM images of aerosols (micron, submicron and nanoparticles) during CO_2 laser processing of polymers

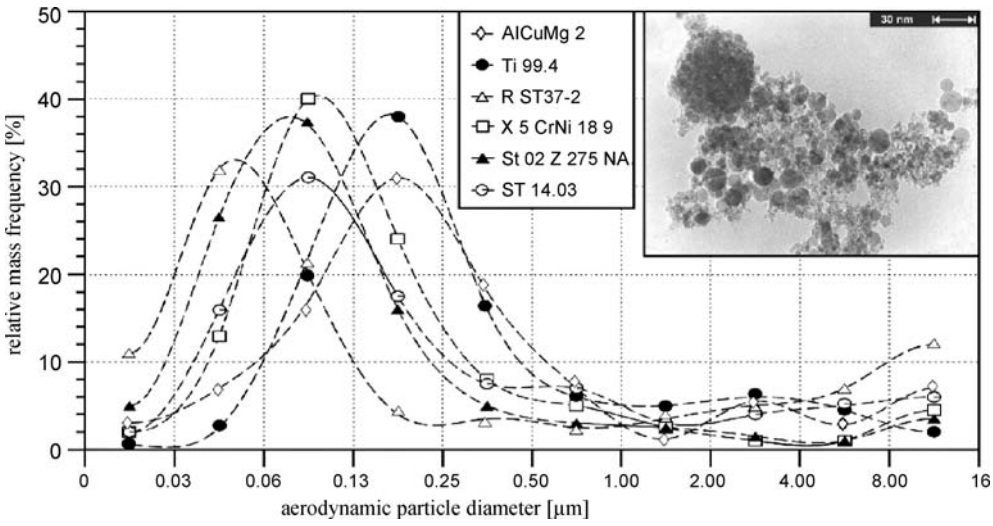

FIGURE 2 Size distributions and SEM image of aerosols (micron, submicron and nanoparticles) during CO_2 laser processing of metals and alloys

in higher or lower thermal impact, these differences in laser parameters do not drastically change the properties of generated nanoparticles.

However, a quite different situation can occur under the use of ultra-short femtosecond (fs) pulsed laser radiation, leading to different physics of laser–matter interaction [41–43]. Indeed, the femtosecond laser ablation is characterized by a variety of novel phenomena, such as: (i) the reduction of the pulse energy that is required to induce ablation at fixed laser wavelength and focusing conditions, (ii) a significant reduction or complete removal of the heat-affected zone (HAZ), (iii) separation in time of laser energy absorption and ablation processes. Recent studies of the femtosecond ablation confirm different properties of nanoparticles compared to longer pulses [44]. In particular, such ablation provides a much higher energy of nanoparticles ejected at narrower angles [45] and allows a much better control of the size and dispersion of nanoparticles produced in water by changing the radiation intensity [26, 46, 47].

In this paper, we examine femtosecond laser ablation from various solid targets in air and water in order to study the properties of nanoparticles that are obtained in typical conditions of femtosecond laser micromachining applications. We also study the influence of processing conditions (pulse energy, micromachining speed) on the characteristics of the produced nanoparticles.

2 Experimental results

The generation of nanoparticles was carried out using a commercial femtosecond laser system (Spectra Physics, Spitfire PRO), delivering 120-fs laser pulses at 800-nm wavelength. This system produces fs pulses with an energy of up to 1 mJ and operates at a repetition rate of 1 kHz. A four-stage positioning unit for laser micromachining by 3D-Micromac was used.

The setup applied to produce nanoparticles in gaseous and liquid media is shown in Fig. 3. A target was placed on the positioning unit. The laser beam was focused by a lens on the target surface. By changing the position of the target, the laser beam can irradiate different parts of the target surface. In our tests, we mainly used silver, titanium, gold and cobalt targets. The experiments in gaseous media were carried out in ambient air. In this case, the released nanoparticle emissions were measured online with an electrical low pressure impactor (ELPI, Dekati), which captures the generated emissions directly after their release. This device contains 12 impaction stages. The particles first pass through a charger, where they are charged electrically. Subsequently, the particles are size-classified by impaction on the particular stage according to their aerodynamic diameter. There, the charged particles produce an electrical current, which is recorded and is converted into the particle number concentration of each size.

Femtosecond laser ablation in liquid media was carried out in an open glass vessel. The material is placed onto the bottom of the glass vessel. The vessel is filled with 2–10 ml liquid. The thickness of the water layer above the target was 3.5 to 18 mm. During the process in liquid media, generated particles are dispersed as colloids.

For the determination of ablation rate, or particle production rate, in gaseous and liquid media, two different methods were used. First, the ablated volume is determined by measuring the three-dimensional ablation geometry generated during the ablation process using microscopy. The second method is carried out by weighing the material before and after the ablation process. The ablation rate results from the difference in mass.

Sizes of the colloid nanoparticles have been measured by transmission electron microscopy (TEM) after drying a colloid droplet at room temperature on the TEM grid (graphite surface).

3 Results

3.1 *Ablation in gaseous environment*

A first series of experiments were focused on the characterization of nanoparticles using femtosecond laser ablation of different metals. We studied the influence of the material, machining speed and pulse energy on the mass of ablated material and the size of the generated particles.

To study the influence of the material on the size of the produced particles, we performed ablation experiments of different materials in air under identical experimental conditions. Figure 4 shows the percentage of nanoparticles from organic, metallic and ceramic materials generated by the femtosecond

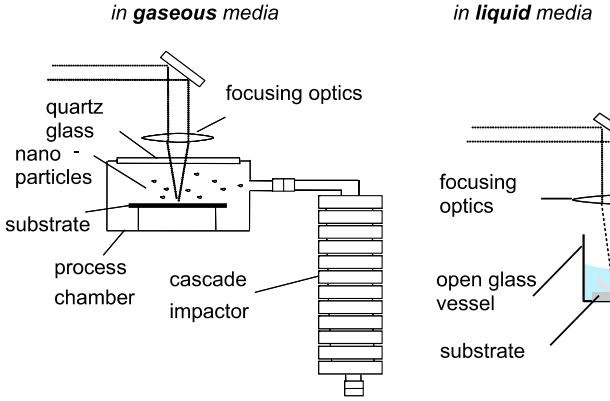

FIGURE 3 Setup of nanoparticle generation in gaseous and liquid media by femtosecond laser ablation of a solid target

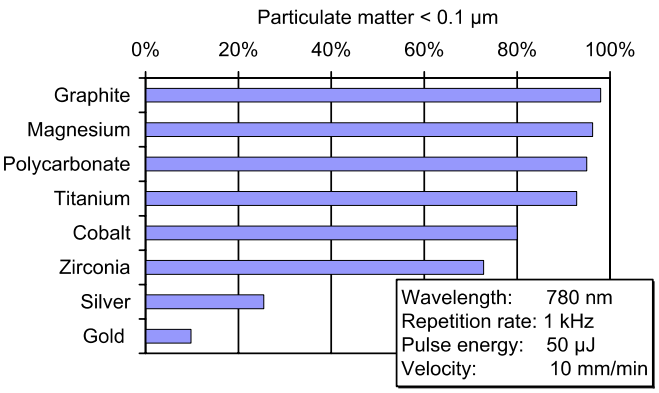

FIGURE 4 Fraction of particles < 100 nm from different materials released during fs laser ablation

laser ablation using identical laser and process parameters. Graphite and magnesium as examples demonstrate the maximal relative number of particulate matter < 100 nm (95%, 98%), while nanoparticles of gold and silver are characterized by a lower share of nanoparticles (10%, 25%) in the generated aerosol. This difference in the size properties for metals and other materials is not yet completely understood. Further investigations are in progress to clarify these results.

Figure 5 shows the influence of the velocity and the laser pulse energy on the ablation rate of titanium and silver. The maximum ablation rate of titanium of 2.2 ng per pulse was achieved using the highest pulse energy of 500 µJ. The ablation rate of silver was much higher, reaching 9 ng per pulse when the pulse energy was 400 µJ. Such a difference in the ablation rates can be explained by the difference in the surface roughness produced by successive laser pulses.

To characterize the velocity (machining speed), it is useful to introduce the parameter of 'pulse overlap', corresponding to the overlap (in percent) of the irradiation spots on the target surface between successive pulses. As follows from Fig. 5, for Ti there is an optimal overlap of 95% (50 mm/min), which provides the highest amount of mass ablation. Similar optimal pulse overlaps of 95% were obtained for Ag (Fig. 5b) and several other materials, suggesting the existence of common optimal conditions for machining speed. We believe that the existence of the optimal overlap reflects the dynamic equilibrium between the following processes: (i) the increase of the radiation absorption due to the appearance of defects on the target surface as a result of the ablation by previous pulses; (ii) the increase of the radiation absorption as a result of an increased incident angle of the laser beam at the premachined spot area (due to the formation of ripples or small spikes); (iii) the decrease of the radiation absorption due to the formation of sufficiently large spikes within the crater as a result of its multipulse ablation [32, 33].

However, our experiments revealed quite different pulse overlap optima for the maximization of production of small nanoparticles. As follows from Fig. 6a, showing the size distribution of nanoparticles of Ti for different pulse overlaps, the increase of the pulse overlap from 78% to 99% leads to the increase of the relative number frequency of nanoparticles in the sub-100-nm range by about 50%. Similar data with the optimum around 99% were obtained for Ag (Fig. 6b).

It has to be emphasized that the frequency of production of sub-60-nm silver particles was lower compared to Ti. Thus, smallest nanoparticles were produced in high overlap numbers using relatively low scanning velocity, corresponding to the ablation of each spot by at least 100 pulses. This significant effect of the pulse overlap on the nanoparticle size distribution has to be taken into account in further investigations.

Laser fluence was considered as an alternative parameter to control the size of nanoparticles formed during femtosec-

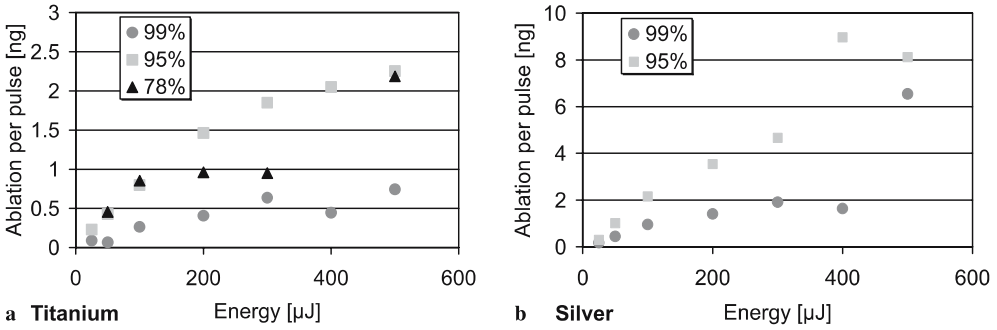

FIGURE 5 Influence of the pulse overlap and energy on the mass ablation per pulse for (**a**) titanium and (**b**) silver in gaseous media

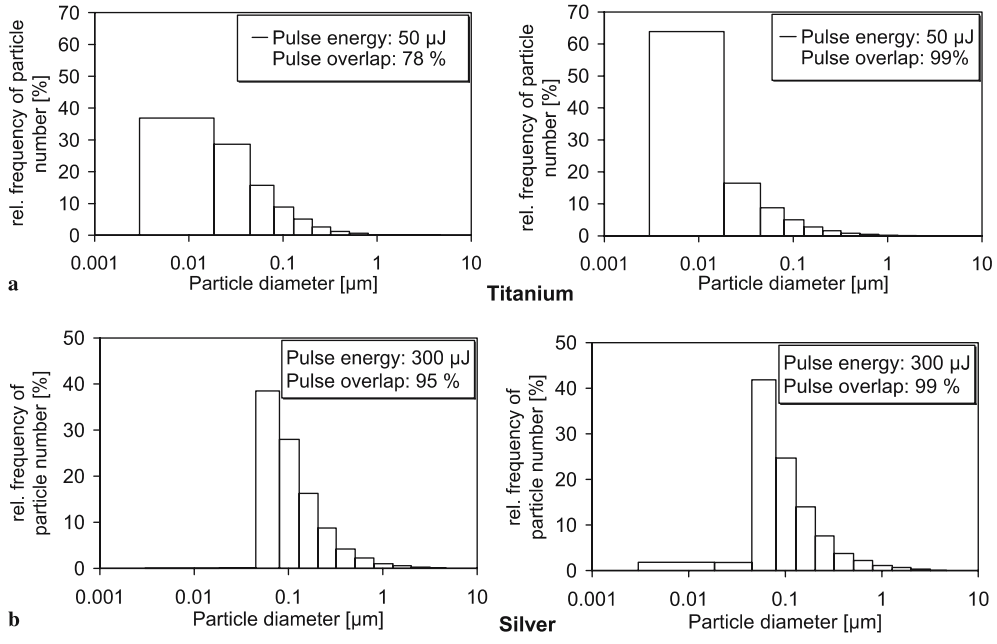

FIGURE 6 Influence of the pulse overlap on the particle size distribution of (**a**) titanium and (**b**) silver

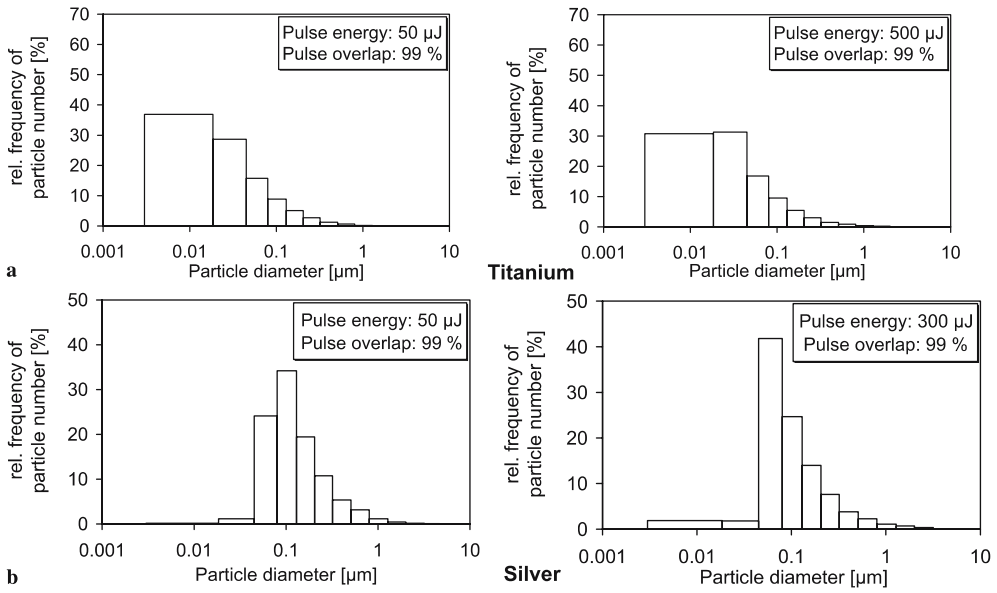

FIGURE 7 Influence of the pulse energy on the particle size distribution of (**a**) titanium and (**b**) silver

ond laser ablation in air. However, we observed only a slight influence of the laser fluence on the nanoparticle size distribution. In particular, as shown in Fig. 7a, a 10-fold increase of the laser fluence from 50 µJ to 500 µJ could not remarkably change the distribution of Ti nanoparticles. Similar minor modifications of the size distribution with a slight increase in the number of particles < 100 nm were observed in the case of Ag at higher laser fluences (Fig. 7b). Although the amount of Ag nanoparticles was relatively low compared to Ti, we could also observe a shift of the distribution maximum from 100 nm to 60 nm at higher laser fluences.

Our results show that mainly the pulse overlap but also the fluence affects the mass rate and distribution of metal (Ag and Ti) nanoparticles generated during femtosecond laser ablation in air. Optimizing these parameters, the production of pure nanoparticles can be controlled even in the absence of external methods of size selection such as cascade impaction. Note that these data differ from the results on femtosecond laser ablation in water [25], which are characterized by a linear log-normal correlation of the nanoparticle size with the laser fluence.

3.2 *Ablation in gaseous environment under pressurized air and water (airbrushing)*

To understand the effect of water on the femtosecond laser ablation-based nanofabrication process, we modified the experimental setup by using a convergent nozzle and a commercial airbrush system supplying pressurized air and air with water into the ablation region. As in Sect. 3.1, we mainly addressed the size distribution of nanoparticles produced during these conditions.

Figure 8a shows the particle size distribution generated by fs laser ablation (50 µJ, 10 mm/min) of a cobalt target. The particle size distribution was measured online (1 Hz) during the quasi-continuous ablation process. More than 80% of the cobalt particles generated in ambient air were in the range of 100–250 nm. The supply of air under pressure (0.12 MPa) to the ablation region via a conical nozzle could suppress particle agglomeration, shifting the majority of particles into the sub-100-nm region. The resulting maximum of the particle number distribution is located at 60 nm. In another experiment, water was added to the pressurized air using the same airbrush kit. Spraying a thin water film on the surface leads to a further reduction of the maximum of the particle size distribution to 30 nm. This method, compared to simple ablation in air, increases the share of cobalt nanoparticles with the diameter ≤ 100 nm from 20% to 90%.

These measurements were repeated with the titanium target, and the same behavior of the particle size distribution was observed (Fig. 8b). In general, with titanium targets smaller particles, as compared to cobalt, are generated during femtosecond laser ablation in air. Supply of air to the ablation region shifts the particle size distribution maximum from 60 nm

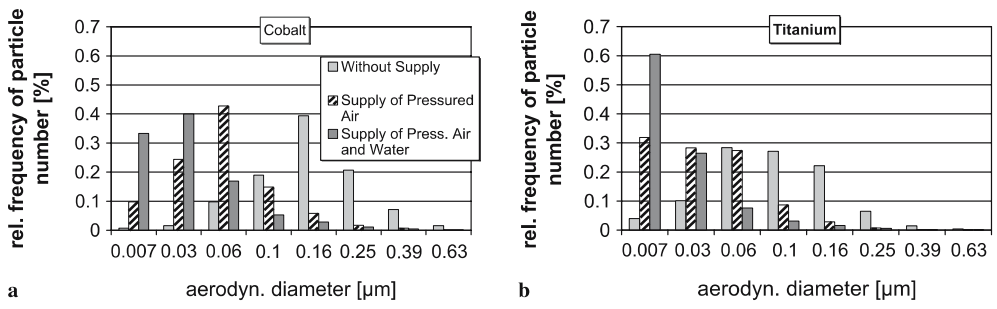

FIGURE 8 Influence of air brushing on the size distribution of (**a**) cobalt and (**b**) titanium particles generated by femtosecond laser ablation in ambient air

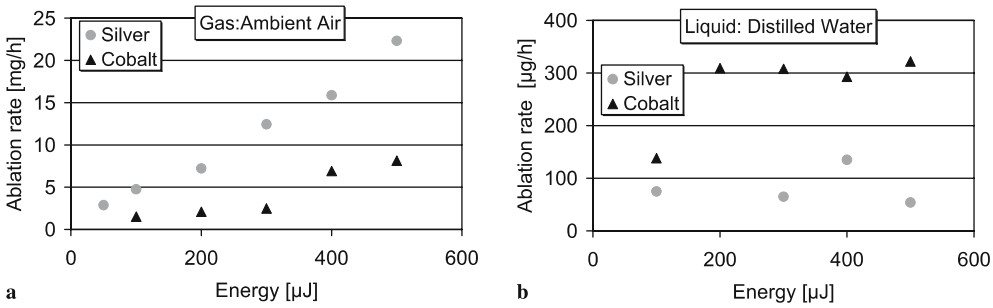

FIGURE 9 Ablation rates of materials in (**a**) gaseous and (**b**) liquid media

to 7 nm. Airbrushing the sample during fs laser processing leads to the production of particles (> 60%) in the 7-nm-size level, and the share of nanoparticles with the diameter ≤ 100 nm increases from 65% to 95%.

Thus, airbrushing of Co or Ti during fs laser ablation in ambient air significantly decreases the average particle size. Moreover, the addition of water to pressurized air leads to a further decrease of nanoparticle size. In general, such methods lead to an increase of the amount of particles smaller than 100 nm or 60 nm by a factor of 2–3. In our opinion, such a high efficiency of nanoparticle size reduction is explained by the decrease of probability of nanoparticle coalescence when pressurized air or air with water is supplied to the ablation region. Indeed, a constant supply of pressurized air quenches the nanoparticle growth by removing nanoparticles from the region of their production and by decreasing the probability of their encounter and coalescence with other particles. The addition of water reinforces the process by a more rapid cooling of nanoparticles and by further quenching of nanoparticle collisions.

3.3 *Ablation in water*

First, the ablation rates of silver, cobalt and gold samples in water were determined. Figure 9 presents a comparison of ablation rates for silver and cobalt in water and air at different laser pulse energies. The ablation rate in water for these materials reaches a maximum at a certain laser fluence and then decreases, whereas the ablation in air is characterized by a gradual increase of the ablation rate with the growing laser fluence. In general, the ablation rate in water appeared to be at least 50-times less efficient. The existence of the saturation and much lower ablation rates in water can be explained by radiation losses in the produced breakdown plasma and by pulse break-up in water before reaching the target [48].

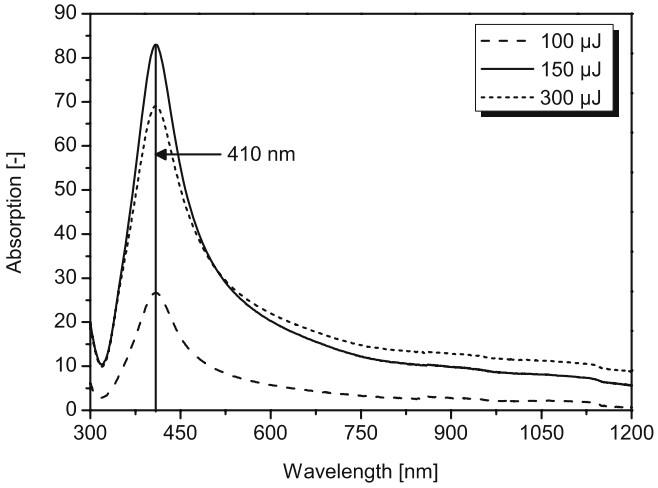

FIGURE 10 Optical characteristics (plasmon resonance) of silver nanoparticles generated by femtosecond laser ablation of silver in water

Our studies showed that the ablation process in liquids is accompanied by a visible coloration of the solution within a few seconds due to the production of nanoparticles. In particular, the solution became yellow-green and red in the cases of Ag and Au targets, respectively. The increase of the laser fluence could also lead to the appearance of metallic tints in the solution under high radiation fluences. As shown in Figs. 10 and 11, absorption spectra from the solutions exhibit peaks at 410–420 and 520–530 nm for Ag and Au, respectively. The appearance of these peaks is generally attributed

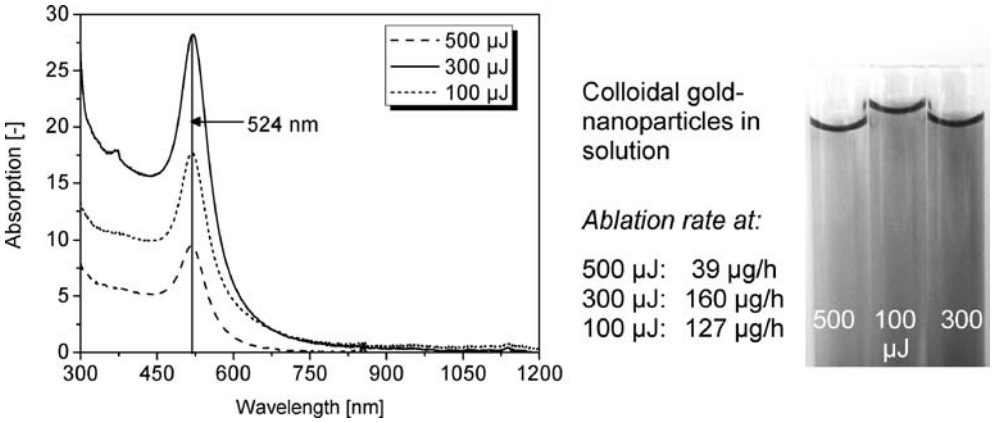

FIGURE 11 Optical characteristics (plasmon resonance), ablation rates and visual appearance of the colloids of gold nanoparticles generated by femtosecond laser ablation of gold in water

to the generation of localized plasmon resonances in metal nanoparticles [49, 50]. It is remarkable that the plasmon-related absorption peaks of the gold and silver colloids have the highest intensity under moderate laser pulse energy. At lower pulse energies, a smaller amount of material is ablated leading to a lower mass concentration of the ablated material and a less intense plasmon resonance signal. The highest plasmon-related absorption peak is achieved using 150-μJ laser pulse energy for Ag and 300 μJ for Au, respectively. Higher laser pulse energies lead to the increase of the mean size of the generated nanoparticles (and size dispersion), resulting in a lower number concentration of nanoparticles at a given ablated mass. This observation is confirmed by SEM images, shown in Fig. 12, which illustrate that with 300-μJ laser pulses the smallest nanoparticles are produced. These data are in agreement with previous results on the femtosecond laser ablation in liquids, which revealed a strong dependence of the nanoparticle size on both laser fluence [25] and the position of the target with respect to the focal point of the lens [46]. Recording of the plasmon resonance spectra, shown in Figs. 10 and 11, was repeated during five weeks without observing any changes in the spectra. Thus, colloids generated during femtosecond laser ablation are highly stable. This is a very important feature, since a shelf life of > 1–2 weeks is often required for the subsequent procedures, e.g. in nanoengineering applications.

Finally, it is important to note that laser ablation in liquids gives much better opportunities to manipulate the size and other properties of nanoparticles. In particular, ablation in liquids enables us to control the size and size dispersion of nanoparticles by the addition of various chemically active compounds into liquid solutions. In this case, the compounds bind to the surface of newly synthesized nanoparticles and, thus, prevent them from coalescencing, drastically reducing the nanoparticle size [26–28]. An example of such a size reduction is shown in Fig. 13. Here, a spectacular reduction of the nanoparticle size is achieved by the use of aqueous solutions of oligosaccharides (β-cyclodextrin) and biopolymers (polyethylene glycol, PEG). In particular, in the case of β-cyclodextrin, the size of the nanoparticles and the size dispersion did not exceed 2.5 nm and 1 nm full width at half maximum (FWHM), respectively.

Laser ablation in water can be used to create a mixture of different nanoparticles without mixing colloids or adding chemical precursors. This mixture can be produced by placing two different targets into the same water reservoir and ablating them sequentially with a femtosecond laser. In this case, a relative concentration of nanoparticles of different materials can be controlled by the processing time of each target. An example of such a mixture, produced from Au and Ag targets, is shown in Fig. 14. The TEM image in this figure shows that gold and silver nanoparticles tend to bind with each other. As shown in the related absorption spectra (Fig. 14), the mixtures simultaneously exhibited two peaks, associated with the plasmon resonances of Au and Ag nanoparticles. The relative intensity of the peaks depends on the number concentration of nanoparticles of each kind. Observing the plasmon resonance at the Ag and Au peak wavelengths, one may easily design a process-control unit which switches the laser beam scanning on the respective target, allowing us to directly control the share of gold and silver nanoparticles in the colloid.

A similar approach can be applied to produce other binary, tertiary or even more complex multimaterial colloids, which is of great interest for various applications in nanoengineering and medicine.

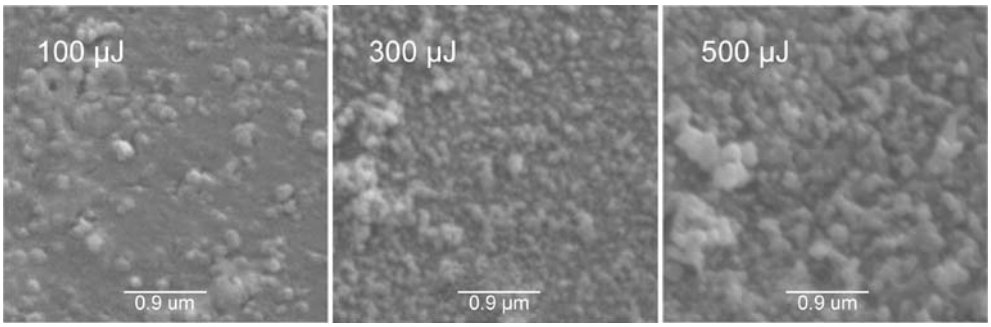

FIGURE 12 SEM photographs of gold nanoparticles generated using different pulse energies

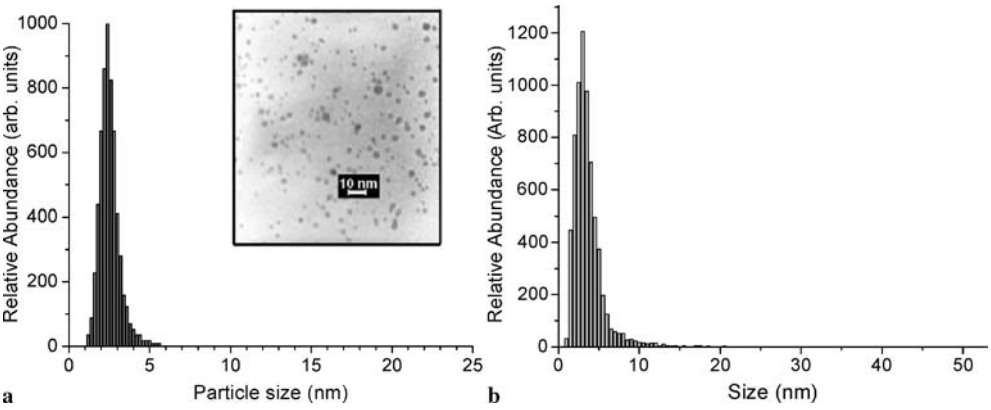

FIGURE 13 TEM images and corresponding size distributions of Au nanoparticles prepared by the fs ablation in oligosaccharides (β-cyclodextrin) (**a**) and biopolymers (polyethylene glycol, PEG) (**b**)

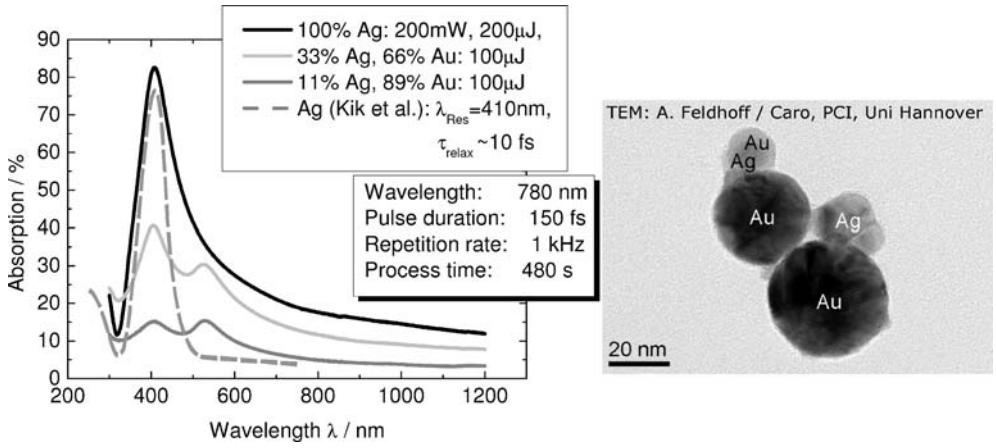

FIGURE 14 Tuning of the Au/Ag nanoparticle concentration and absorption spectra by sequential fs laser ablation of Ag and Au in the same water sample. Reference spectrum [51] from Kik et al.

4 Conclusions

In summary, femtosecond laser ablation in typical micromachining conditions has been studied as a tool for the fabrication of various nanomaterials. It has been found that this kind of ablation leads to an effective synthesis of nanoparticles, which appear as airborne nanoparticles (aerosols) and nanoparticles dispersed in liquids (colloids) under experiments in air and water, respectively.

Femtosecond laser ablation experiments performed in air with eight different materials have shown that the ablated material in the cases of graphite and magnesium contains the highest percentage of nanoparticles (95–98%). Using identical laser and process parameters, the generated gold and silver aerosols are characterized by a significantly lower share of nanoparticles (15–25%).

It has been demonstrated that femtosecond laser ablation in a gaseous environment is characterized by an up to 10 times higher ablation rate compared to laser ablation in water, whereas the size and optical properties of the manufactured nanoparticles can be affected by changing the pulse overlap and laser fluence.

During the generation of nanoparticulate aerosols, it has been demonstrated for the first time, to the best of our knowledge, that the increase of the pulse overlap leads to a significant (50%) increase in the amount of fs laser generated nanoparticles.

A compromise between the laser ablation in water and air environments is represented by the nanoparticle generation using the airbrushing method. In this case, a higher productivity of nanoparticles (than in water) and smaller sizes (than in air) have been demonstrated. Airbrushing and water supply lead to an increase of the amount of particles smaller than 60 nm by a factor of three.

Despite much lower production rates, laser ablation in water and aqueous solutions gives much better opportunities to manipulate the size, size dispersion and other properties of colloids. In particular, this kind of ablation can be used to synthesize nanoparticles with a small mean size and low size dispersion, and to form ultra-pure colloidal nanoparticles without using any chemical precursors or additives which may have adverse effects on the biocompatibility. Moreover, the generation of a stable Ag-Au colloid by sequential ablation in the same reservoir has been studied as an approach toward multimaterial nanoparticle dispersions.

Because of this purity, controllable size and possible multimaterial design, nanoparticles produced by femtosecond laser ablation can be promising for biomedical applications (e.g. Ag, Cu, Ti nanoparticles) embedded in polymers [51, 52].

ACKNOWLEDGEMENTS The work was supported by the Laboratory of Nano and Quantum Engineering (LNQE) of the University of Hannover, Germany. The authors would like to thank A. Feldhoff and J. Caro for the TEM analysis of gold and silver nanoparticles.

REFERENCES

1 A. Ebenau, in *Nanotechnology in Chemistry – Experience Meets Vision*, Mannheim, 28–29 October 2002 (BASF Future Business GmbH, Ludwigshafen, 2002), press release
2 P.T. Anastas, J.C. Warner, *Green Chemistry: Theory and Practice* (Oxford University Press, New York, 1998)
3 T.-H. Her, R.J. Finlay, C. Wu, S. Deliwala, E. Mazur, Appl. Phys. Lett. **73**, 1673 (1998)
4 C.H. Crouch, J.E. Carey, J.M. Warrender, M.J. Aziz, E. Mazur, F.Y. Genin, Appl. Phys. Lett. **84**, 1850 (2004)
5 A.J. Pedraza, J.D. Fowlkes, D.H. Lowndes, Appl. Phys. Lett. **74**, 2322 (1999)
6 F. Costache, M. Henyk, J. Reif, Appl. Surf. Sci. **186**, 352 (2002)
7 F. Korte, J. Serbin, J. Koch, A. Egbert, C. Fallnich, A. Ostendorf, B.N. Chichkov, Appl. Phys. A **77**, 229 (2003)
8 F. Korte, J. Koch, B.N. Chichkov, Appl. Phys. A **79**, 879 (2004)
9 J. Koch, F. Korte, T. Bauer, C. Fallnich, A. Ostendorf, B.N. Chichkov, Appl. Phys. A **81**, 325 (2005)
10 A.V. Kabashin, M. Meunier, Appl. Phys. Lett. **82**, 1619 (2003)
11 A.V. Kabashin, M. Meunier, Mater. Sci. Eng. B **101**, 60 (2003)
12 D.-Q. Yang, A.V. Kabashin, V.-G. Pilon-Marien, E. Sacher, M. Meunier, J. Appl. Phys. **95**, 5722 (2004)
13 A.V. Kabashin, M. Meunier, in *Recent Advances in Laser Processing of Materials*, ed. by J. Perriere, E. Millon, E. Fogarassi (Elsevier, Amsterdam, 2006), pp. 1–36
14 I.A. Movtchan, R.W. Dreyfus, W. Marine, M. Sentis, M. Autric, G. Le Lay, N. Merk, Thin Solid Films **255**, 286 (1995)
15 Y. Yamada, T. Orii, I. Umezu, S. Takeyama, T. Yoshida, Japan. J. Appl. Phys. **35**, 1361 (1996)
16 T. Makimura, Y. Kunii, K. Murakami, Japan. J. Appl. Phys. **35**, 4780 (1996)
17 A.V. Kabashin, J.-P. Sylvestre, S. Patskovsky, M. Meunier, J. Appl. Phys. **91**, 3248 (2002)
18 A. Fojtik, A. Henglein, Ber. Bunsenges. Phys. Chem. **97**, 252 (1993)
19 J. Nedderson, G. Chumanov, T.M. Cotton, Appl. Spectrosc. **47**, 1959 (1993)
20 F. Mafuné, J.-Y. Kohno, Y. Takeda, T. Kondow, H. Sawabe, J. Phys. Chem. B **104**, 9111 (2000)

21 F. Mafuné, J.-Y. Kohno, Y. Takeda, T. Kondow, J. Phys. Chem. B **105**, 5114 (2001)
22 Y.-H. Chen, C.S. Yeh, Colloid Surf. A **197**, 133 (2002)
23 T. Tsuji, K. Iryo, N. Watanabe, M. Tsuji, Appl. Surf. Sci. **202**, 80 (2002)
24 S.I. Dolgaev, A.V. Simakin, V.V. Voronov, G.A. Shafeev, F. Bozon-Verduraz, Appl. Surf. Sci. **186**, 546 (2002)
25 A.V. Kabashin, M. Meunier, J. Appl. Phys. **94**, 7941 (2003)
26 A.V. Kabashin, M. Meunier, C. Kingston, J.H.T. Luong, J. Phys. Chem. B **107**, 4527 (2003)
27 J.-P. Sylvestre, A.V. Kabashin, E. Sacher, M. Meunier, J.H.T. Luong, J. Am. Chem. Soc. **126**, 7176 (2004)
28 J.-P. Sylvestre, S. Poulin, A.V. Kabashin, E. Sacher, M. Meunier, J.H.T. Luong, J. Phys. Chem. B **108**, 16 864 (2004)
29 J. Muramoto, Y. Nakata, T. Okada, M. Maeda, Japan. J. Appl. Phys. **36**, L563 (1997)
30 D.B. Geohegan, A.A. Puretzky, G. Duscher, S.J. Pennycook, Appl. Phys. Lett. **73**, 438 (1998)
31 D.B. Geohegan, A.A. Puretzky, G. Duscher, S.J. Pennycook, Appl. Phys. Lett. **72**, 2987 (1998)
32 S.R. Foltyn, in *Pulsed Laser Deposition of Thin Films*, ed. by D.B. Chrisey, G.K. Hubler (Wiley, New York, 1994), Chap. 4 and references therein
33 D.J. Krajnovich, J.E. Vazquez, J. Appl. Phys. **73**, 3001 (1993)
34 F.F. Abraham, *Homogeneous Nucleation Theory: The Pretransition Theory of Vapor Condensation* (Academic, New York, 1974)
35 D. Kashchiev, *Nucleation: Basic Theory with Applications* (Butterworth-Heinemann, Oxford, 2000)
36 M. Goede, VDI Rep., Ser. 5, No. 587 (VDI, Düsseldorf, 2000)
37 First International Symposium on High-Power Laser Macroprocessing, ed. by I.M. Miyamoto, K.F. Kobayashi, K. Sugioka, R. Poprawe, H. Helia-jian, Proceedings of the SPIE, Volume 4831 (2003), pp. 459–462
38 J. Koch, A. von Bohlen, R. Hergenröder, K. Niemax, J. Anal. Atom. Spectrom. **19**, 267 (2004)
39 A. Ostendorf, S. Barcikowski, T. Püster, J. Bunte, in *Tagung Optische Technologien in der Kunststofftechnik*, Munich, 11–12 November 2003 (VDI Rep. No. 1810) (VDI, Düsseldorf, 2003), pp. 113–130
40 S. Barcikowski, R. Ostrowski, J. Marczak, M. Strzelec, J. Walter, A. Ostendorf, in *Laser Cleaning II*. ed. by D.M. Kane (World Scientific, Singapore, 2006), Chapt. 9, pp. 197–208
41 S. Preuss, A. Demchuk, M. Stuke, Appl. Phys. A **63**, 315 (1996)
42 T. Götz, M. Stuke, Appl. Phys. A **64**, 539 (1997)
43 I. Zergioti, M. Stuke, Appl. Phys. A **67**, 391 (1998)
44 J. Bunte, S. Barcikowski, T. Puester, T. Burmester, M. Brose, T. Ludwig, in *Femtosecond Technology for Technical and Medical Applications*, ed. by F. Dausinger et al. (Springer Top. Appl. Phys. **96**) (Springer, Berlin, 2004), Chap. 9.2, pp. 309–321
45 J. Perrière, E. Millon, W. Seiler, C. Boulmer-Leborgne, V. Craciun, O. Albert, J.C. Loulergue, J. Etchepare, J. Appl. Phys. **91**, 690 (2002)
46 J.-P. Sylvestre, A.V. Kabashin, E. Sacher, M. Meunier, Appl. Phys. A **80**, 753 (2005)
47 S. Besner, J.-Y. Degorce, A.V. Kabashin, M. Meunier, Appl. Surf. Sci. **247**, 163 (2005)
48 A. Vogel, J. Noack, K. Nahen, D. Theisen, S. Busch, U. Parlitz, D.X. Hammer, G.D. Noojin, B.A. Rockwell, R. Birngruber, Appl. Phys. B **68**, 271 (1999)
49 M. Kerker, *The Scattering of Light and Other Electromagnetic Radiation* (Academic, New York, 1969)
50 U. Kreibig, M. Vollmer, *Optical Properties of Metal Clusters* (Springer, Berlin, 1996)
51 P.G. Kik, S.A. Maier, H.A. Atwater, Mater. Res. Soc. **705**, Y3.6.1 (2002)
52 J.R. Morones, J.L. Elechiguerra, A. Camacho, K. Holt, J.B. Kouri, J.T. Ramirez, M.J. Yacaman, Nanotechnology **16**, 2346 (2005)